

Journal of Biomedical Optics

BiomedicalOptics.SPIEDigitalLibrary.org

Fully automated muscle quality assessment by Gabor filtering of second harmonic generation images

Rik Paesen
Sophie Smolders
José Manolo de Hoyos Vega
Bert O. Eijnde
Dominique Hansen
Marcel Ameloot

Fully automated muscle quality assessment by Gabor filtering of second harmonic generation images

Rik Paesen,^a Sophie Smolders,^a José Manolo de Hoyos Vega,^a Bert O. Eijnde,^{a,b} Dominik Hansen,^{a,b} and Marcel Ameloot^{a,*}

^aHasselt University, Biomedical Research Institute, Agoralaan Building C, 3590 Diepenbeek, Belgium

^bHasselt University, REVAL–Rehabilitation Research Center, Agoralaan Building A, 3590 Diepenbeek, Belgium

Abstract. Although structural changes on the sarcomere level of skeletal muscle are known to occur due to various pathologies, rigorous studies of the reduced sarcomere quality remain scarce. This can possibly be explained by the lack of an objective tool for analyzing and comparing sarcomere images across biological conditions. Recent developments in second harmonic generation (SHG) microscopy and increasing insight into the interpretation of sarcomere SHG intensity profiles have made SHG microscopy a valuable tool to study microstructural properties of sarcomeres. Typically, sarcomere integrity is analyzed by fitting a set of manually selected, one-dimensional SHG intensity profiles with a supramolecular SHG model. To circumvent this tedious manual selection step, we developed a fully automated image analysis procedure to map the sarcomere disorder for the entire image at once. The algorithm relies on a single-frequency wavelet-based Gabor approach and includes a newly developed normalization procedure allowing for unambiguous data interpretation. The method was validated by showing the correlation between the sarcomere disorder, quantified by the M-band size obtained from manually selected profiles, and the normalized Gabor value ranging from 0 to 1 for decreasing disorder. Finally, to elucidate the applicability of our newly developed protocol, Gabor analysis was used to study the effect of experimental autoimmune encephalomyelitis on the sarcomere regularity. We believe that the technique developed in this work holds great promise for high-throughput, unbiased, and automated image analysis to study sarcomere integrity by SHG microscopy. © 2016 Society of Photo-Optical Instrumentation Engineers (SPIE) [DOI: [10.1117/1.JBO.21.2.026003](https://doi.org/10.1117/1.JBO.21.2.026003)]

Keywords: striated muscle; second harmonic generation; screening; supramolecular model.

Paper 150661R received Oct. 4, 2015; accepted for publication Jan. 15, 2016; published online Feb. 5, 2016.

1 Introduction

Various types of muscle diseases with changes on the sarcomere level have been identified,¹ including types of distal muscular dystrophy, which are often caused by defects in structural components of sarcomeres.² However, myopathy-related research is seldom based on the study of sarcomeres. Instead, myofiber cross-sections are considered to detect irregularities or odd features such as nemalin rods,³ and to study changes in cross-sectional area due to myogenesis or muscle atrophy.^{4,5} For these studies, standard tools, such as immunohistochemistry (IHC), are used to stain and visualize specific proteins within the tissue. In case sarcomeres are considered, structural details of the sarcomere organization is obtained by transmission electron microscopy (TEM). Both IHC and TEM rely on tedious sample preparation. IHC requires many staining optimization steps, while TEM might suffer from possibly biased human selection of representative regions.⁶ Therefore, these standard techniques do not allow study of sarcomere irregularities in a high-throughput fashion. The development of a fast and reliable screening tool of sarcomere morphology would be very helpful.

Label-free second harmonic generation (SHG) microscopy provides an attractive pathway that can meet these conditions. Because of the extreme high degree of ordering of the myosin thick filaments, strong SHG signals arise from skeletal muscle

tissue,^{7–11} making SHG a perfect tool for imaging sarcomeric structures. Muscle degradation is known to be related to disruption of M-proteins, which interconnect thick filaments to attain sarcomere integrity.^{12,13} The thick filament misalignment due to absence of M-proteins is known to lie at the basis of clear transition from normal single-band to double-band SHG intensity profiles.^{8,14} Based on a supramolecular sarcomere model to calculate the expected SHG intensity profiles, the degree of thick filament misalignment can be quantified by means of an apparent increase in the centrosymmetric M-band size.^{8,14} Currently, this degree of sarcomere disorder is mostly obtained by analyzing local, manually selected one-dimensional sarcomere intensity profiles. On the other hand, based on the distance-dependent correlation value of the gray-level co-occurrence matrix, Liu et al.¹⁵ suggested a method for assessing sarcomere regularity of an entire SHG image. Their approach yields a reliable quantitative measure for sarcomere quality, but produces only a single value to describe the complete manually selected area containing multiple sarcomeres.

For assessing the muscle quality by analysis of full SHG images of muscle tissue while preserving local information, we designed a specific algorithm based on Gabor analysis.¹⁶ In general, the Gabor analysis relies on wavelets to obtain local frequency content and orientation information.^{16,17} This approach is referred to as Gabor decomposition and has been applied in a broad range of applications in the field of computer

*Address all correspondence to: Marcel Ameloot, E-mail: marcel.ameloot@uhasselt.be

vision technology.^{18,19} In the work by Recher et al.,⁹ a bifrequency Gabor-based approach was already introduced to locate single- and double-band SHG patterns of manually selected one-dimensional sarcomere intensity profiles. Here we propose to use an alternative Gabor approach in which regular, single-band sarcomeres are located by analyzing full images for the frequency related to the average sarcomere length. Sarcomere irregularities such as double-band SHG patterns, but also so-called pitchforks,^{9,20} or any other type of anomaly will predominantly be described by higher-frequency components and hence become automatically detected as the remainder of this single-frequency detection. This makes a full Gabor decomposition redundant and substantially speeds up the analysis. In the current study, we introduce a fully automated and fast muscle quality assessment tool based on this single-frequency Gabor analysis, yielding a per pixel so-called Gabor value to quantify the sarcomere integrity. The analysis includes a new normalization procedure, allowing for easy sarcomere comparison across various imaging platforms and biological conditions. Moreover, the procedure is designed in such a way that image processing such as cropping to representative regions, image rotation, and noise reduction is unnecessary.

The newly introduced Gabor analysis is used to study muscle deterioration due to experimental autoimmune encephalomyelitis (EAE), an animal model to study the effects of demyelination in the context of multiple sclerosis (MS).²¹ Central nervous system (CNS) deficit as a consequence of MS is known to result in decreased central motor function, leading to muscle weakness,^{22,23} and ultimately decreased muscle activity. Muscle disuse is known to induce atrophy,²⁴ for which changes on the sarcomere level can occur.²⁵ To study the relation between EAE severity and sarcomere regularity, muscle tissue from EAE-induced rats and healthy rats is compared. First, the data are used to indicate how the Gabor values should be interpreted based on representative SHG intensity profiles. Next, the relation between the disorder-related M-band size^{8,14} and the normalized Gabor value is studied to justify the use of the Gabor approach for assessing sarcomere regularity. Finally, we study the correlation between the EAE severity and the sarcomere regularity quantified by our normalized Gabor value.

2 Materials and Methods

2.1 Experimental Autoimmune Encephalomyelitis Rat Model

Flexor digitorum longus (FDL) muscle samples were isolated from 8- to 10-week-old residual female Dark Agouti rats. Rats were purchased from Harlan Netherlands B.V. (Horst, The Netherlands). Experiments were conducted in accordance with institutional guidelines and approved by the Ethical Committee for Animal Experiments of Hasselt University.

EAE was induced by a subcutaneous injection at the base of the tail with a 200 μ l solution composed of 140 μ g of recombinant human myelin oligodendrocyte glycoprotein in complete Freund's adjuvant (F5506, Sigma-Aldrich, St. Louis, Missouri) supplemented with 2.5 mg/ml H37RA heat-inactivated *Mycobacterium tuberculosis* (Difco, BD Diagnostics, Maryland). Healthy control animals did not receive any injection. Immunized rats were weighed and received a pain score (PS) on a daily basis according to the following neurological scale: 0.5 = partial loss of tail tonus, 1 = complete loss of tail tonus,

2 = hind limb paresis, 3 = hind limb paralysis, 4 = moribund, 5 = death.²⁶ EAE rats were sacrificed 30 days after immunization.

2.2 Tissue Preparation

All animals were sacrificed by heart perfusion with Ringer solution after Nembutal injection (100 mg/kg). FDL muscles were immediately removed from both hind limbs, incubated overnight in 4% para-formaldehyde at 4°C, followed by cryoprotection in 30% sucrose in phosphate buffered saline (PBS) at 4°C until the tissue had sunk. Muscles were frozen in optimal cutting temperature compound (Tissue-Tek, Sakura Finetek Europe, The Netherlands) using liquid nitrogen cooled isopentane and stored at -80°C. Sections of thickness 14 μ m were cut on a cryostat (CL 1990 UV, Leica, Wetzlar, Germany) along the length of the myocytes, mounted onto Superfrost Plus glasses (Menzel-Gläser, Thermo Fisher Scientific, Waltham, Massachusetts), and stored at -20°C. Before imaging, sections were washed thrice for 5 min in PBS, dipped into milli-Q, and a coverslip was placed using Immu-Mount™ (Thermo Fisher Scientific). Coverslipped sections were stored at 4°C until imaging.

2.3 Microscopy

SHG imaging was performed using a Zeiss LSM510 META (Carl Zeiss, Jena, Germany) mounted on an Axiovert 200M and a 20 \times /0.75 air objective (Plan-Apochromat 20 \times /0.75, Carl Zeiss). The excitation was provided by a femtosecond pulsed laser (MaiTai DeepSee, Spectra-Physics, California) tuned at a central wavelength of 810 nm. The SHG signal was collected in forward mode by a condenser with a numerical aperture (NA) of 0.55, which we have verified to be sufficient to collect the complete SHG emission profile using the supramolecular sarcomere model.⁸ After passing through a 400 to 410 nm bandpass filter, the signal was detected by an analogue photomultiplier tube, delivered by Zeiss.

2.4 Sarcomere Profile Analysis

Sarcomere analysis based on manually selected profiles was done as previously described.¹⁴ In short, 2728 intensity profiles were manually selected from 68 SHG images, taken from both healthy ($n = 5$) and EAE ($n = 8$) animals. Each profile was analyzed using the supramolecular model developed by Rouède et al.,⁸ yielding the sarcomere length L and the disorder-related M-band size M . Based on our previous observations, the analysis was done using an A-band length of $A = 1.40 \mu$ m, a refractive index (RI) at the illumination wavelength $n_{\omega} = 1.39$, and an RI at the SHG wavelength $n_{2\omega} = 1.41$.¹⁴ For the selected objective, the Gaussian point spread function (PSF) has a lateral size of $w_{xy} = 0.59 \mu$ m and an axial size of $w_z = 3.45 \mu$ m (half width at e^{-2}).¹⁴

2.5 Gabor Analysis

In general, a Gabor analysis is used to obtain local frequency components in a signal, either in time or in space. In this work, we consider the SHG images of striated muscle as a spatial signal. The main spatial frequency f present in these SHG images of regular sarcomeres is related to the sarcomere length L , such that $f = L^{-1}$. The purpose of the algorithm is to locate and quantify sarcomere anomalies at the pixel level. Since SHG images of sarcomere anomalies are typically characterized by

spatial frequency components f' other than f , our algorithm was designed to obtain a local quantifier indicating the relative contribution of f to the signal, which we refer to as the local Gabor value. Regions consisting of regular sarcomeres will then receive the highest possible Gabor value.

Instead of a relative contribution, a standard Gabor analysis returns the absolute contribution of the considered frequency. Hence, regions containing similarly appearing sarcomeres will have undesired differing Gabor values if the signal intensity differs. These intensity variations are likely to occur not only across samples but also within a sample due to variations in a real sample's thickness or changes in opacity of features above and below the focal plane. To obtain a relative quantifier, we implemented a new normalization procedure, which yields a normalized Gabor value $\bar{G}(x, y)$.

In Appendix A, we give the theory on which our approach is based. In short, the normalized Gabor value is defined as

$$\bar{G}(x, y) = 2 \frac{|G^f(x, y) * I(x, y)|}{A(x, y)}, \quad (1)$$

where $*$ is the convolution product, $I(x, y)$ is the experimental image data, $A(x, y)$ is the oscillation amplitude related to local SHG intensities [see Eq. (3) in Appendix A], and

$$G^f(x, y) = \frac{3f^2}{2\pi} \exp\left(-\frac{f^2x^2}{2} - \frac{9f^2y^2}{2} + 2\pi ifx\right) \quad (2)$$

is the Gabor kernel. This approach was implemented in a fully automated analysis algorithm, which requires only the image as input. The algorithm is described in Appendix B.

2.6 Computing System

The Gabor analysis was performed on a standard 64-bit PC with a 3.6 GHz quad core processor, extended with an Nvidia GeForce GTX 680 graphical processing unit (GPU). The analysis code was written in MATLAB® (Version R2013a, The Mathworks, Natick, Massachusetts), and the parallel processing toolbox was used for its built-in GPU capabilities.

2.7 Simulations

Theoretical SHG intensity profiles were simulated using the supramolecular model developed as described before.¹⁴ The one-dimensional profiles were calculated along the x -direction by the supramolecular model and copied laterally (y -direction) to obtain two-dimensional images. Gaussian noise resembling that of the used imaging modality was superimposed onto the theoretical profiles. The PSF, refractive indexes, and A-band length were fixed to the previously mentioned values. The sarcomere length was fixed to $L = 2.2 \mu\text{m}$.

2.8 Statistics

Data comparison over different conditions was done using the one-way analysis of variance algorithm of MATLAB®'s statistical toolbox. Differences were considered significant for $p < 0.001$. Data correlation was tested by MATLAB®'s *corrcoef* function, which, besides correlation, returns the probability p of incidental correlation. Correlation was taken to be significant for $p < 0.05$.

3 Results

3.1 Typical Patterns and Their Gabor Values

To correctly interpret the resulting Gabor values, the Gabor histograms of representative sarcomere structures and anomalies are given in Fig. 1. In Figs. 1(a) and 1(b), the difference between the original and normalized Gabor values, respectively, is shown for the same regular sarcomeres. Without normalization, the

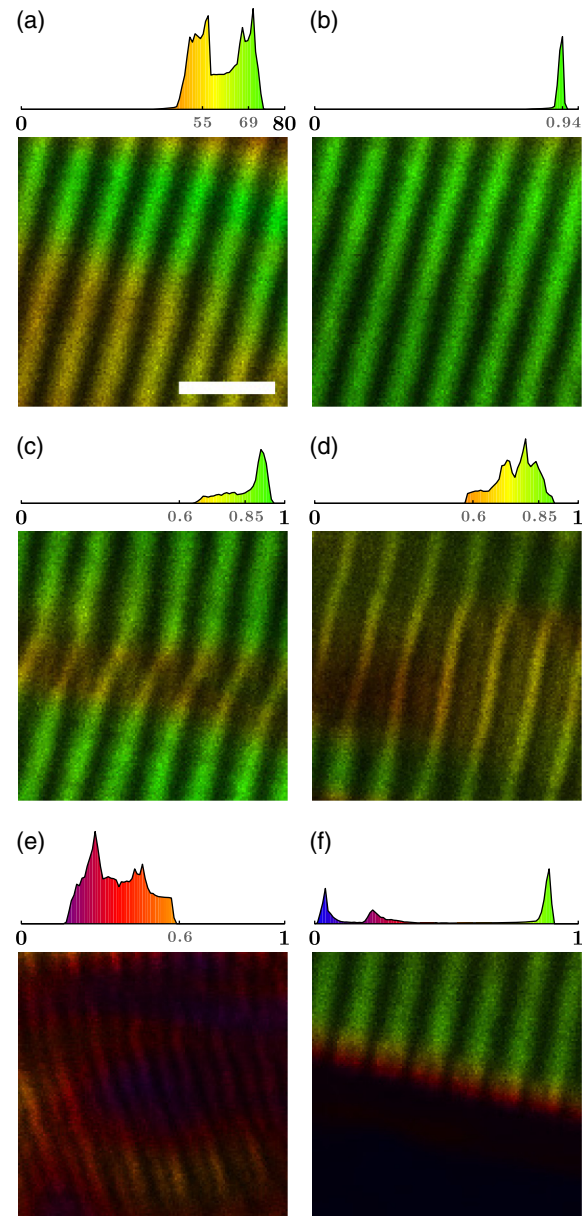


Fig. 1 Typical results of the suggested Gabor filter. The color map represents the Gabor value, as specified in the histogram above each image. Each panel shows a cropped region of a larger image containing background regions. (a) Typical proper sarcomere pattern without normalization [$G(x, y)$] and (b) the same data as (a) with normalization [$\bar{G}(x, y)$]. In panels (c) to (f), the normalized Gabor coefficient is shown. Typical irregularities such as (c) pitchforks and (d) thinned regions show a slight decreased normalized Gabor value. Other typical structures contributing to the Gabor histogram of an image are: (e) double-band regions and (f) edge effects and dark regions (no mask applied for illustrative purposes). Scale bar $5 \mu\text{m}$. All images have the same field of view.

Gabor distribution contains two distinct peaks with a central value of ~ 69 and ~ 55 , which is a 20% difference. The distinct peaks suggest the image contains structures with different frequencies. However, a one-dimensional fast Fourier transform (FFT) analysis along the sarcomeres indicates that the frequency mismatch is only apparent (data not shown). The FFT reveals a peak having a width representing a 2.5% frequency spread, corresponding to a 1% normalized Gabor value decrease according to Eq. (9). After normalization [Fig. 1(b)], the Gabor histogram contains only one peak at an average value of 0.932. The standard deviation of 0.018 matches a 2% spread and resembles the mismatch deduced from the FFT analysis. This typical example shows the explicit need for the normalization procedure. From here on, only the normalized Gabor values (\bar{G}) are considered.

A first type of anomaly that can be detected using the normalized Gabor analysis is a pattern where the signal appears to come from one half of the thick filament [Figs. 1(c)–1(d)]. In these structures, often referred to as pitchforks,⁹ the A-band splits into two smaller myosin regions. One of these two regions typically has a higher SHG intensity. Pitchforks can occur on both short [Fig. 1(c)] or longer transversal length scales [Fig. 1(d)]. However, the Gabor values are independent of this length scale and consistently range from ~ 0.6 in the center of the pattern to >0.85 near the fully formed sarcomeres.

A second type of anomaly is the double band pattern, which was suggested in previous studies as a typical feature for proteolytic muscle tissue.^{8,9} The double-band features result in lower Gabor values, down to a normalized Gabor value of 0.08 when the pattern contains only this doubled frequency. In most cases, the double-band pattern contains a combination of the reference frequency f and the doubled frequency, resulting in Gabor values ranging from 0 to 0.6 [Fig. 1(e)].

The last representative pattern is a technical artifact rather than a sarcomere anomaly. SHG images of sarcomeres will contain myocyte boundaries and background (dark) regions that are also analyzed by the protocol [Fig. 1(f)]. However, these image regions do not contain valuable information on the sarcomere regularity. Therefore, the boundary and background regions are excluded from the Gabor histogram by the mask defined in Appendix B, eliminating the additional histogram peaks near $\bar{G} = 0$.

In general, all aforementioned patterns contribute to the final Gabor histogram, which represents the sarcomere regularity in the entire SHG image. It appears that a Gabor value below 0.6 always maps disordered sarcomeres. Values between 0.6 and 0.85 indicate myocyte alterations related to an increasing or decreasing number of sarcomeres, indicated by the presence of pitchforks.⁹ Finally, values above 0.85 will always represent regular sarcomere patterns and are considered as good and healthy regions.

3.2 Gabor Value Correlates with Myosin Disorder

In order to link the obtained \bar{G} to sarcomere disorder, the correlation between the normalized Gabor value and the M-band size was studied. This was done on a set of samples taken from healthy animals and EAE induced animals for which sarcomere degradation was expected. A broad range of values for M was obtained by analyzing manually selected intensity profiles from samples of both animal groups. The automatically determined normalized Gabor value corresponding to each profile was taken from the pixel at the profile center. For each intensity profile, \bar{G} is plotted against the corresponding M in Fig. 2.

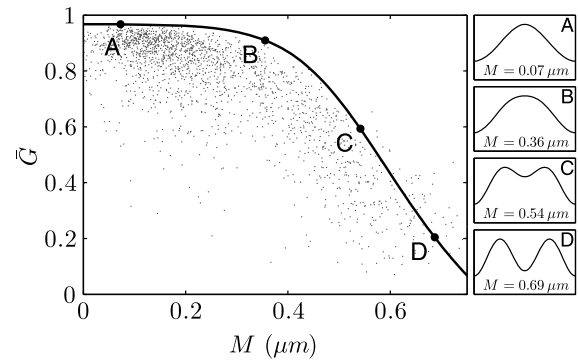


Fig. 2 Sarcomere disorder quantified by M versus normalized Gabor value \bar{G} correlation. The maximum possible normalized Gabor value is indicated by the solid line (simulated). The simulated profiles of the given M-band size are shown on the right.

For $M < 0.3 \mu\text{m}$, the normalized Gabor value is essentially constant, indicating no detectable change in the SHG profile. Above this threshold value, a transition from single to double band occurs, resulting in a rapid decrease of \bar{G} . A correlation between M and \bar{G} exists, validating the applicability of our Gabor approach to automatically estimate sarcomere (ir)regularity from entire SHG images. The observed $M - \bar{G}$ correlation was additionally verified by means of simulations. For each M-band size, images containing only one type of sarcomere were simulated in accordance with experimental conditions and analyzed with the normalized Gabor approach. The resulting maximum possible \bar{G} for each M , shown by the solid line in Fig. 2, clearly indicates the upper limit of the experimental data. The simulations show that the Gabor approach is less sensitive to small M-band sizes, while for $0.3 < M < 0.75$, the method is highly sensitive.

3.3 Experimental Autoimmune Encephalomyelitis Affects Sarcomere Integrity

Using the Gabor histograms, the effect of EAE on sarcomere integrity was studied. For this, the global EAE severity of each animal is measured by the pain score averaged from the day of EAE induction to the day of sample collection ($\langle PS \rangle$). The data used in Sec. 3.2 were divided into three groups: a healthy control group ($n = 5$), animals with a time-averaged pain score below 1 ($\langle PS \rangle < 1$, $n = 5$), referred to as mild EAE, and animals with a time-averaged pain score above 1 ($\langle PS \rangle > 1$, $n = 3$), referred to as severe EAE. For each animal, the Gabor histograms of four to six SHG images from different slices were combined, resulting in one Gabor histogram per animal. These histograms, combined per animal group, are shown in Fig. 3 (histograms per animal are shown in Appendix C).

Relative to the control group, the Gabor histogram shifts toward lower values only for the severe EAE group. According to previous observations (Fig. 1), this shift is mainly due to transformation from regular single-band SHG patterns into double-band patterns. The control, mild EAE, and severe EAE histogram cross at values representative for pitchfork structures (see Fig. 1), indicating little or no change in their prevalence. The mild EAE group shows no clear difference with respect to the control group. Only small differences are observed at $\bar{G} > 0.85$, for which no sarcomere alterations were assumed. Moreover, statistical comparison of the median normalized Gabor values ($\bar{G}_{1/2}$, see upper axis in Fig. 3) shows no

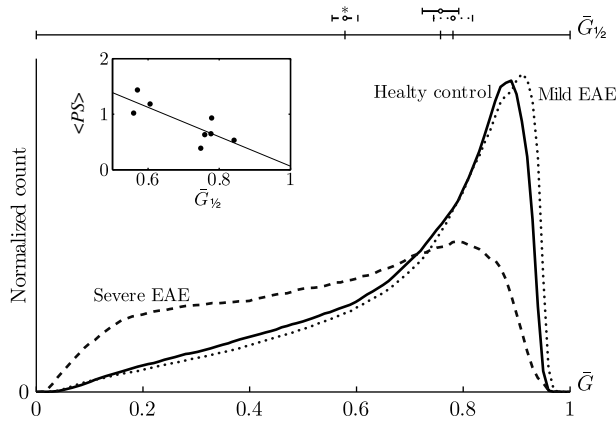


Fig. 3 Gabor histograms of healthy control group ($n = 5$), the mild EAE group ($n = 5$), and the severe EAE group ($n = 3$). As indicated on the upper horizontal axis, a significantly lower median Gabor value ($\bar{G}_{1/2}$) for the severe EAE group is observed (*, $p < 0.001$). The inset shows the correlation between $\bar{G}_{1/2}$ and the time average pain score ((PS)). The solid line is a linear fit serving as a guideline to emphasize this correlation.

significant difference between both groups. Only the severe EAE group has a significantly lower $\bar{G}_{1/2}$ ($p < 0.001$) relative to both the control and mild EAE group.

The fact that severe EAE results in lower median normalized Gabor values than mild EAE suggests that a correlation exists between the EAE pain score on which data grouping was based and the muscle quality assessed by the Gabor analysis. To emphasize this correlation, the time-averaged EAE pain score ((PS)) is compared to the median Gabor value of each animal. The result is shown in the inset in Fig. 3. A correlation analysis reveals a correlation coefficient of -0.81 ($p < 0.05$), indicating a strong relation between the average pain score and the median Gabor value.

4 Discussion and Conclusions

We introduced a new and automated method based on Gabor analysis to accurately characterize the sarcomere quality from an SHG microscopy image of skeletal muscle. Instead of performing a full Gabor decomposition, we chose to analyze the image with only one frequency that is related to the sarcomere length and give interpretation to the resulting normalized Gabor values. First, the Gabor values can be linked to typical sarcomere SHG profiles, either regular structures giving rise to single-band profiles or any of the discussed anomalies that are detectable by SHG microscopy (Fig. 1). Second, we showed that the resulting Gabor values relate to sarcomere disorder quantified by the M-band size, giving a structural meaning to the Gabor values. Compared to the analysis of manually selected profiles, previously used to obtain the same structural information, the Gabor method is objective and extremely fast. Our fully automated sarcomere integrity mapping requires only the image as input, provided that it contains a preferential sarcomere direction and a background region. The analysis occurs in <5 s for a 2048×2048 8-bit image using a GPU. Moreover, the method gains information on the entire image instead of just a few manually selected intensity profiles.

We believe that the newly introduced normalization method forms the strength of the proposed Gabor analysis. Normalization makes the interpretation of the results independent of imaging properties, such as illumination power or

detector gain; also, local intensity variations due to opacity properties of tissue above and below the scanning plane are circumvented.

We assumed that all sarcomeres are contracted similarly such that sarcomere length is the same for all sarcomeres, including possibly irregular ones. Moreover, we have not studied the relation between sarcomere integrity and sarcomere length. One could anticipate that for increasing sarcomere length, the base frequency has a lower relative contribution for well-ordered sarcomeres because the A-band length remains constant. Since \bar{G} estimates this relative contribution, longer sarcomeres will yield lower normalized Gabor values, even for well-ordered sarcomeres. The normalized Gabor approach thus needs to be revised when considering samples with longer sarcomeres.

This study was limited to images taken with an objective having a moderate NA of 0.75. If one would prefer a higher resolution, in spite of our recommendation to use moderate NA objectives,¹⁴ typical sarcomere anomalies (Fig. 1) might be characterized by different normalized Gabor values. Moreover, the $M - \bar{G}$ relation (Fig. 2) might alter. For regular sarcomeres, this can be expected due to the more pronounced shoulder regions.¹⁴ These shoulder regions are described by higher harmonics, causing a lower relative contribution of the base frequency, and thereby a lower \bar{G} . Additional work is thus needed to use the approach presented in this work for images obtained through elevated NA objectives.

When introducing the theoretical background of our Gabor approach, we considered SHG intensity oscillations as a single harmonic function with the base frequency related to the sarcomere length. This is not in accordance with the model developed by Rouède et al.⁸ Consequently, the normalized Gabor value will never reach its maximum value of 1, as can also be observed from the simulation results shown in Fig. 2. The maximum normalized Gabor value approaches $\bar{G} \approx 0.97$ for regular profiles ($M \approx 0$), meaning that $\sim 97\%$ of the profile consists out of the base frequency. By inspection of the amplitude spectrum of the SHG profile calculated by the supramolecular model, we found that 98% of the profile is represented by the base frequency. This indicates that the normalized Gabor value closely resembles the expected value given by the supramolecular model. Moreover, the simplified phenomenological model is an acceptable 3% off for regular sarcomeres, making our Gabor approach ideal to locate regular, and therefore irregular, sarcomeres.

Note that at a given M , experimental values of \bar{G} are mainly lower than the theoretical maximum estimated from simulations (Fig. 2). This might be a consequence of the single frequency approach, which does not cope with small variations in the sarcomere contraction state. Moreover, manually selected profiles might be located close to anomalies, which could slightly affect the Gabor values at the profile site due to the lateral kernel dimension σ_y .

We have not thoroughly tested the effect of the imaging noise level on the normalized Gabor values. Yet, because of the selected kernel size, spatial noise will be Gaussian averaged over a range of pixels, improving the signal-to-noise ratio by a factor of ~ 40 relative to the original imaging noise. Conversely, this approach overlooks irregularities occurring on length scales of individual sarcomeres. However, our approach is still more sensitive to local variations than, for instance, the gray-level co-occurrence matrix method described by Liu et al.,¹⁵ in which the complete selected region is represented

by a single oscillating profile. And although we similarly propose to condense the full Gabor image into a single histogram for easy interpretation, the local information remains present in the initial Gabor analyzed images and can always be referred to.

The applicability of our new Gabor analysis was tested in the context of EAE induced muscle degradation. To our knowledge, this is the first time SHG microscopy was used to assess sarcomere quality in an EAE study. We showed that the Gabor histograms represent sufficient information to compare the different biological conditions. A significant decrease of the median Gabor value is observed for the severe EAE animals with an average pain score above 1. As these animals typically showed multiple relapses before sample collection (data not shown), the number of relapses seems to have an effect on muscle quality. Based on these results, we can, however, not state that the decreased muscle quality is a direct consequence of muscle disuse. EAE is known as an inflammatory disease of the CNS, and the resulting systemic inflammatory signals mediate the skeletal muscle metabolism, eventually resulting in muscle atrophy.²⁷ As each relapse coincides with an increased inflammatory state,²⁸ the observed relation between number of relapses through the average pain score and the muscle quality suggests, indeed, that muscle atrophy is related to CNS inflammation rather than muscle disuse. Although additional work is required to prove this statement, the observed relation seems to suggest that relapsing-remitting EAE might not be an appropriate model for studying MS-related sarcomere alterations.

In our study, only rat muscle samples were used for the verification and application of the new Gabor approach. However, because striations are typical for skeletal muscle of all vertebrates, and because of a low variability of the sarcomere architecture among vertebrate species,²⁹ the Gabor analysis can be directly applied to study skeletal muscle of other vertebrates. This makes the analysis applicable in human studies or in a more clinical context.

Appendix A: Gabor-Based Protocol

In order to explain the design of the Gabor-based protocol, we start by describing a real SHG image of striated muscle tissue using a phenomenological model. This model is based on the assumption that a sample of striated muscle contains only sarcomeres of length L , oriented along the x -direction, such that the base frequency equals $f = L^{-1}$. Due to the intensity variations related to local changes in sample thickness or opacity, the SHG image $I(x, y)$ was modeled with spatially varying amplitude $A(x, y) \geq 0$ and offset $O(x, y) \geq 0$, such that

$$I(x, y) = O(x, y) + A(x, y)\{1 + \cos[2\pi f'(x, y)x]\}, \quad (3)$$

where $f'(x, y)$ is the main local frequency component. For simplicity, the sarcomere SHG intensity was modeled by a harmonic function instead of using the comprehensive model developed by Rouède et al.⁸ According to their model, a regular sarcomere profile consists for 98% out of the base frequency f for the used imaging parameters. This makes Eq. (3) a good approximation of regular SHG profiles for which $f'(x, y) = f$. Anomalies are then dominated by the local frequency $f'(x, y) \neq f$, up to $f'(x, y) \approx 2f$ for double-band patterns.

A practical implementation of the Gabor transform is based on the two-dimensional (2-D) convolution of an image with a Gabor kernel. To obtain the local contribution of the frequency f , the Gabor kernel is defined as³⁰

$$G^f(x, y) = \frac{1}{2\pi\sigma_x\sigma_y} \exp\left(-\frac{x^2}{2\sigma_x^2} - \frac{y^2}{2\sigma_y^2} + 2\pi ifx\right), \quad (4)$$

where σ_x and σ_y are the widths of the kernel in the x and y directions, respectively. Due to the position-frequency uncertainty,¹⁶ the width along the sarcomere direction is a crucial parameter for the sensitivity of the analysis. For $\sigma_x \gg f^{-1}$, a high-frequency accuracy is obtained with a low positional accuracy, while the opposite holds for $\sigma_x \ll f^{-1}$. A good trade-off for frequency matching and localization is valid when $\sigma_x \approx f^{-1}$, for which the kernel spans about three sarcomere units (see side panels of step 3 in Fig. 4). The choice of σ_y is not related to the length of the sarcomeres. The value of σ_y defines the smallest lateral length scale on which changes are detectable. This length is already limited by the PSF of the imaging device. This PSF size can be estimated using the Rayleigh criterion.³¹ Yet, using the PSF size to set σ_y requires additional input parameters to the Gabor analysis. Alternatively, we can assume that lateral changes typically occur on a length scale of one sarcomere, such that $\sigma_y \approx \sigma_x/3$. For most imaging systems, this value is higher than the PSF size, but it will prove to be sufficiently small to detect sarcomere irregularities. The Gabor kernel can then be rewritten as

$$G^f(x, y) = \frac{3f^2}{2\pi} \exp\left(-\frac{f^2x^2}{2} - \frac{9f^2y^2}{2} + 2\pi ifx\right). \quad (5)$$

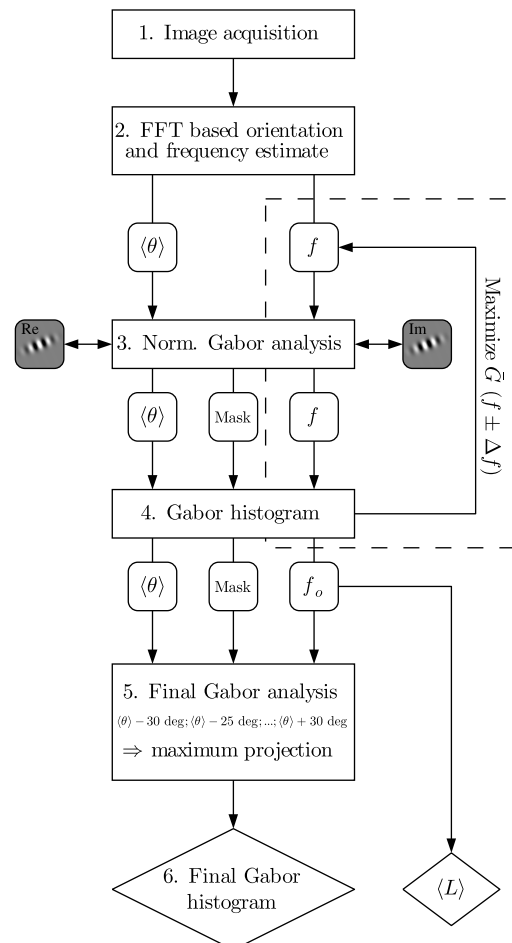


Fig. 4 Automated Gabor analysis flowchart.

In our study, the Gabor analysis was applied by first convolving the full image with the Gabor kernel of frequency f related to the average sarcomere length and then taking the modulus ($|\dots|$) of this convolution product (*).

$$G(x, y) = |G^f(x, y) * I(x, y)|. \quad (6)$$

The resulting value $G(x, y)$ is defined as the local Gabor value. If $A(x, y)$, $O(x, y)$, and $f'(x, y)$ are slowly varying with respect to f^{-1} , then evaluating Eq. (6) results in

$$\begin{aligned} G(x, y) \approx & \frac{A(x, y)}{2} \left| \exp[2\pi i f'(x, y)x] \right. \\ & \times \exp\left\{ -\frac{[f'(x, y) - f]^2}{2\left(\frac{f}{2\pi}\right)^2} \right\} + 2 \exp(-2\pi^2) \\ & + \frac{2O(x, y)}{A(x, y)} \exp(-2\pi^2) \\ & \left. + \exp[-2\pi i f'(x, y)x] \exp\left\{ -\frac{[f'(x, y) + f]^2}{2\left(\frac{f}{2\pi}\right)^2} \right\} \right|. \quad (7) \end{aligned}$$

The three last terms are negligibly small compared to the first term for nonzero oscillation amplitude $A(x, y)$, such that

$$G(x, y) \approx \frac{A(x, y)}{2} \exp\left\{ -\frac{[f'(x, y) - f]^2}{2\left(\frac{f}{2\pi}\right)^2} \right\}. \quad (8)$$

The local Gabor value thus comprises both the amplitude $A(x, y)$ and the frequency mismatch $f'(x, y) - f$ of the sarcomere related intensity oscillation. We introduce a normalization procedure to compensate for the amplitude variation due to instrumental or sample related artifacts, such that only the local frequency contribution is represented by the Gabor value. The normalized Gabor value $\bar{G}(x, y)$ is defined as

$$\bar{G}(x, y) = 2 \frac{|G^f(x, y) * I(x, y)|}{A(x, y)}. \quad (9)$$

This normalized Gabor value ranges from 0 for complete frequency mismatch to 1 for perfect frequency matching relative to f , independent of the oscillation amplitude and offset. The local amplitude and offset are obtained from the image by solving the system

$$S(x, y) = I(x, y) * |G^f(x, y)|, \quad (10)$$

$$\Sigma(x, y) = I(x, y)^2 * |G^f(x, y)|. \quad (11)$$

Basically, the operations shown in Eqs. (10) and (11) represent a Gaussian smoothing of the experimental image $I(x, y)$, which is only done sufficiently for $f \approx f'$ such that multiple sarcomeres are covered by the smoothing kernel. Combining Eqs. (3) and (5), Eqs. (10) and (11) yield

$$S(x, y) = O(x, y) + A(x, y), \quad (12)$$

$$\Sigma(x, y) = [O(x, y) + A(x, y)]^2 + \frac{A(x, y)^2}{2}. \quad (13)$$

From these, the resulting local amplitude and offset are calculated as

$$A(x, y) = \sqrt{2[\Sigma(x, y) - S(x, y)^2]}, \quad (14)$$

$$O(x, y) = S(x, y) - A(x, y). \quad (15)$$

Thus, by inserting the experimental image $I(x, y)$ into Eqs. (10) and (11), Eqs. (14) and (15) can be used to locally estimate the amplitude and offset of the experimental data.

Appendix B: Automated Analysis Work Flow

A detailed flowchart of the analysis is shown in Fig. 4. The procedure is developed to attain minimal human input throughout the entire analysis. After acquiring the SHG image (step 1), the mean sarcomere orientation $\langle \theta \rangle$ with respect to the horizontal edge of the image and frequency related to the main sarcomere length are estimated. Both frequency and orientation are contained in the first noncentral peak of the 2-D frequency spectrum obtained by FFT of the full image (step 2). First, the frequency coordinate of this spectral peak is detected in a range defined by the typical physiological sarcomere working range, being 1.6 to 3 μm .³² At this frequency f , the angular peak position is determined and taken as the main sarcomere orientation $\langle \theta \rangle$. Both f and $\langle \theta \rangle$ are initial estimates that will be refined later in the procedure. Based on these initial values for frequency and orientation, the initial Gabor kernel is calculated using Eq. (5) including a rotational basis transformation. The real (Re) and imaginary (Im) parts of a typical kernel are shown in step 3 of Fig. 4 for illustrative purposes. The resulting Gabor kernel is applied to the image by a convolution, and additionally, the normalization procedure is performed as described in Appendix A.

For easy data interpretation, all normalized Gabor values belonging to myocytes are condensed into a histogram (step 4). Values of pixels not belonging to sarcomeres, such as areas in between myocytes, are excluded from the histogram by applying a mask. This mask is obtained by considering $O(x, y)$, which takes larger values than the dark noise level at regions containing sarcomeres. The average dark noise level is estimated for each image \mathcal{I} by increasing i , starting at the lowest pixel value, until

$$\text{med}(\mathcal{I}_{\mathcal{I} \leq i-1}) \leq \text{med}(\mathcal{I}_{\mathcal{I} \leq i}), \quad (16)$$

where $\text{med}(\mathcal{I}_{\mathcal{I} \leq i})$ represents the median of pixel values of \mathcal{I} having intensity lower than or equal to i . Considering the image intensity histogram, dark regions induce a local maximum at low intensity values, which is located by this algorithm. Only pixels obeying $O(x, y) > i$ are used to create the Gabor histogram.

Using the histogram resulting from step 4, a frequency optimization routine is performed before continuing to step 5. This optimization is needed to cope with possible variations of sarcomere lengths due to different contraction states at the time of sample preparation. A first estimate of the sarcomere length was obtained by the FFT method in step 2. For each image, the optimal frequency (f_o), related to the average sarcomere length $\langle L \rangle$ present in the image, is obtained by maximizing the 90th percentile normalized Gabor value. By considering a percentile, multiple Gabor values are simultaneously taken into account

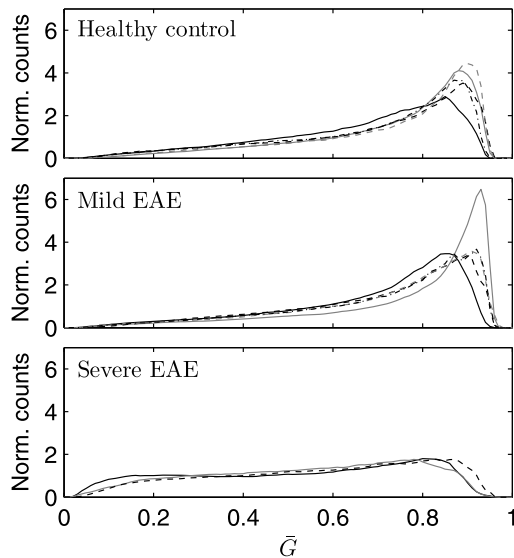


Fig. 5 Gabor histograms per studied animal, grouped per condition.

for frequency optimization, which is not the case when only the maximal Gabor value would be maximized. The optimization is done by repeating steps 3 and 4 with six different frequencies near the initial frequency: $f \pm 7\%$, $f \pm 14\%$, and $f \pm 20\%$. In this, it is assumed that error on the initial estimate of f by the FFT method is maximum 20%, falling within the earlier mentioned physiological sarcomere working range. The resulting seven values are sufficient to perform a second-order polynomial regression, for which the frequency at the polynomial peak is set as the optimal frequency f_o for the considered image. Due to the restriction to the physiological working range of sarcomere lengths, f_o will always represent the main sarcomere length, even when only double-band patterns are present in the image.

In step 5, the actual Gabor analysis is performed with the previously obtained average orientation $\langle\theta\rangle$ and optimal frequency f_o . However, to allow for local changes in orientation, the Gabor kernel is applied for angles ranging from $\langle\theta\rangle - 30$ deg to $\langle\theta\rangle + 30$ deg with a step size of 5 deg. When the kernel orientation matches that of the sarcomere, the Gabor value is maximal. This maximum value is selected for each pixel. This procedure is referred to as maximum projection in Fig. 4. Finally, the resulting Gabor data are condensed into the final Gabor histogram (step 6).

Appendix C: Gabor Histograms Per Animal

In Fig. 5, the Gabor histograms are shown for each animal, grouped per condition. For the healthy group, five animals were used; five animals are contained in the mild EAE group, and three animals are contained in the severe EAE group.

Acknowledgments

We would like to thank Dr. Stelios Ravanidis and Professor Niels Hellings for providing us the muscle samples, and Dr. Leen Slaets for sharing her insights concerning the EAE rat model. This research is part of the Interreg EMR IV-A project BioMiMedics (www.biomimedics.org) and is co-financed by the European Union, local governments, research institutes, and SMEs. Support by the BELSPO funded IAP-PAI network

P7/05 on Functional Supramolecular Systems (FS2) is acknowledged. The Province of Limburg (Belgium) is acknowledged for the financial support within the tUL IMPULS FASE II program, allowing for the upgrading of the laser source used in this work.

References

1. N. G. Laing, Ed., *The Sarcomere and Skeletal Muscle Disease*, Springer, New York (2008).
2. B. Udd, "Molecular biology of distal muscular dystrophies—sarcomeric proteins on top," *Biochim. Biophys. Acta—Mol. Basis Dis.* **1772**(2), 145–158 (2007).
3. D. Sanoudou and A. H. Beggs, "Clinical and genetic heterogeneity in nemaline myopathy—a disease of skeletal muscle thin filaments," *Trends Mol. Med.* **7**(8), 362–368 (2001).
4. T. Fukunaga et al., "Muscle volume is a major determinant of joint torque in humans," *Acta Physiol. Scand.* **172**(4), 249–255 (2001).
5. B. Moss et al., "Effects of maximal effort strength training with different loads on dynamic strength, cross-sectional area, load-power and load-velocity relationships," *Eur. J. Appl. Physiol. Occup. Physiol.* **75**(3), 193–199 (1997).
6. S. M. Wilson and A. Bacic, "Preparation of plant cells for transmission electron microscopy to optimize immunogold labeling of carbohydrate and protein epitopes," *Nat. Protoc.* **7**, 1716–1727 (2012).
7. V. Nucciottia et al., "Probing myosin structural conformation in vivo by second-harmonic generation microscopy," *Proc. Natl. Acad. Sci.* **107**, 7763–7768 (2010).
8. D. Rouède et al., "Modeling of supramolecular centrosymmetry effect on sarcomeric SHG intensity pattern of skeletal muscles," *Biophys. J.* **101**, 494–503 (2011).
9. G. Recher et al., "Three distinct sarcomeric patterns of skeletal muscle revealed by SHG and TPEF microscopy," *Opt. Express* **17**, 19763–19777 (2009).
10. S. V. Plotnikov et al., "Characterization of the myosin-based source for second-harmonic generation from muscle sarcomeres," *Biophys. J.* **90**, 693–703 (2006).
11. P. J. Campagnola and L. M. Loew, "Second-harmonic imaging microscopy for visualizing biomolecular arrays in cells, tissues and organisms," *Nat. Biotechnol.* **21**, 1356–1360 (2003).
12. I. Agarkova et al., "M-band: a safeguard for sarcomere stability?" *J. Muscle Res. Cell Motil.* **24**(2–3), 191–203 (2003).
13. S. Lange et al., "The sarcomeric M-band during development and in disease," *J. Muscle Res. Cell Motil.* **26**(6–8), 375–379 (2005).
14. R. Paesen et al., "On the interpretation of second harmonic generation intensity profiles of sarcomere," *J. Biomed. Opt.* **20**(8), 086010 (2015).
15. W. Liu, N. Raben, and E. Ralston, "Quantitative evaluation of skeletal muscle defects in second harmonic generation images," *J. Biomed. Opt.* **18**(2), 026005 (2013).
16. H. G. Feichtinger and T. Strohmer, Eds., *Advances in Gabor Analysis*, Birkhauser, Boston (2002).
17. S. Grigorescu, N. Petkov, and P. Kruijzinga, "Comparison of texture features based on Gabor filters," *IEEE Trans. Image Process.* **11**, 1160–1167 (2002).
18. V. K. Pothos, C. Theoharatos, and G. Economou, "A local spectral distribution approach to face recognition," *Comput. Vis. Image Underst.* **116**(6), 663–675 (2012).
19. N. Subbanna et al., "Hierarchical probabilistic Gabor and MRF segmentation of brain tumours in MRI volumes," *Lec. Notes Comput. Sci.* **8149**, 751–758 (2013).
20. C. S. Garbe et al., "Automated multiscale morphometry of muscle disease from second harmonic generation microscopy using tensor-based image processing," *IEEE Trans. Biomed. Eng.* **59**(1), 39–44 (2012).
21. R. Furlan, C. Cuomo, and G. Martino, "Animal models of multiple sclerosis," in *Neural Cell Transplantation*, D. Gordon and N. J. Scolding, Eds., Vol. **549**, pp. 157–173, Humana Press, New York (2009).
22. A. V. Ng et al., "Functional relationships of central and peripheral muscle alterations in multiple sclerosis," *Muscle Nerve* **29**(6), 843–852 (2004).

23. J. A. Kent-Braun et al., "Strength, skeletal muscle composition, and enzyme activity in multiple sclerosis," *J. Appl. Physiol.* **83**(6), 1998–2004 (1997).
24. M. L. Urso, "Disuse atrophy of human skeletal muscle: cell signaling and potential interventions," *Med. Sci. Sports Exerc.* **41**(10), 1860–1868 (2009).
25. J. Heslinga, G. te Kronnie, and P. Huijting, "Growth and immobilization effects on sarcomeres: a comparison between gastrocnemius and soleus muscles of the adult rat," *Eur. J. Appl. Physiol. Occup. Physiol.* **70**(1), 49–57 (1995).
26. J. Bogie et al., "Myelin-phagocytosing macrophages modulate autoreactive T cell proliferation," *J. Neuroinflammation* **8**(1), 85 (2011).
27. T. P. Braun et al., "Central nervous system inflammation induces muscle atrophy via activation of the hypothalamic pituitary adrenal axis," *J. Exp. Med.* **208**(12), 2449–2463 (2011).
28. S. F. G. Zorzella-Pezavento et al., "Persistent inflammation in the CNS during chronic EAE despite local absence of IL-17 production," *Mediators Inflammation* **2013**, 10 (2013).
29. S. L. Hooper, K. H. Hobbs, and J. B. Thuma, "Invertebrate muscles: thin and thick filament structure; molecular basis of contraction and its regulation, catch and asynchronous muscle," *Prog. Neurobiol.* **86**(2), 72–127 (2008).
30. T. S. Lee, "Image representation using 2D Gabor wavelets," *IEEE Trans. Pattern Anal. Mach. Intell.* **18**, 959–971 (1996).
31. S. Inoué and K. R. Spring, *Video Microscopy: The Fundamentals (The Language of Science)*, Plenum, New York (1997).
32. T. Burkholder and R. Lieber, "Sarcomere length operating range of vertebrate muscles during movement," *J. Exp. Biol.* **204**(9), 1529–1536 (2001).

Biographies for the authors are not available.